Supplementary materials

Table S1 Simulated input parameters of each functional layer of Sb_2S_3 solar cell with perovskite nanogaps

Reference	Thickness/ nm	Width/nm	Band gap/eV	Electron affinity/eV	Dielectric permittivity (relative)	CB effective density of states, N_c/cm^{-3}	VB effective density of states, N_v/cm^{-3}
Spiro-MeOTAD [1, 2]	80	——	3	2.2	3	2.2×10^{18}	1.8×10^{19}
$MAPbI_3$ [2, 3]	400 (nanogaps)/ 40 (Non-nanogaps)	50	1.59	4.2	6.5	1.66×10^{19}	5.41×10^{19}
Sb_2S_3 [2, 4]	400	500	1.65	3.7	7	2×10^{19}	1×10^{19}
TiO_2 [1]	100	——	3.28	4	9	2×10^{18}	1×10^{19}

Reference	Electron mobility/ (cm^2·V^{-1}·s^{-1})	Hole mobility/ (cm^2·V^{-1}·s^{-1})	Donor concentration, N_d/cm^{-3}	Acceptor concentration, N_a/cm^{-3}	Total defeats concentration, N_t/cm^{-3}	Radiative recombination coefficient, B_{rad}/(cm^3·s^{-1})	Auger recombination coefficient, (A_n/A_p)/(cm^6·s^{-1})
Spiro-MeOTAD [1, 2]	2.1×10^{-3}	1.39×10^{-4}	—	1×10^{18}	1×10^{16}	—	—
$MAPbI_3$ [2, 3]	0.38	0.65	—	1×10^{15} (nanogaps)/ 1×10^{18} (non-nanogaps)	1×10^{15}	3.27×10^{-11}	0.88×10^{-29}
Sb_2S_3 [2, 4]	10	2.6	—	1×10^{15}	1×10^{18}	—	—
TiO_2 [1]	20	10	1.0×10^{17}	—	1×10^{16}	—	—

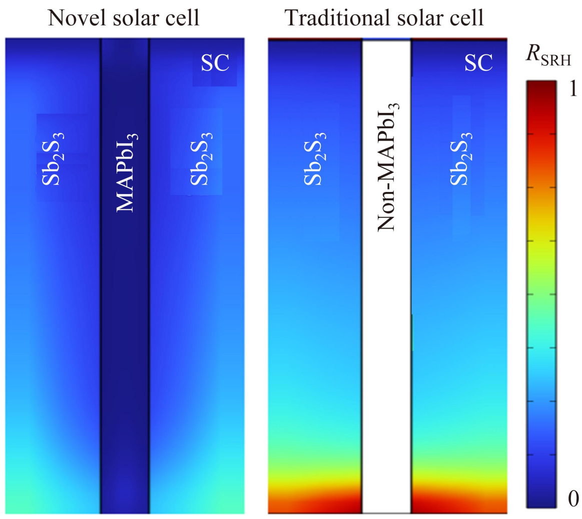

Figure S1 Normalized SRH recombination rate (R_{SRH}) distribution profiles of the novel and traditional Sb_2S_3 solar cells

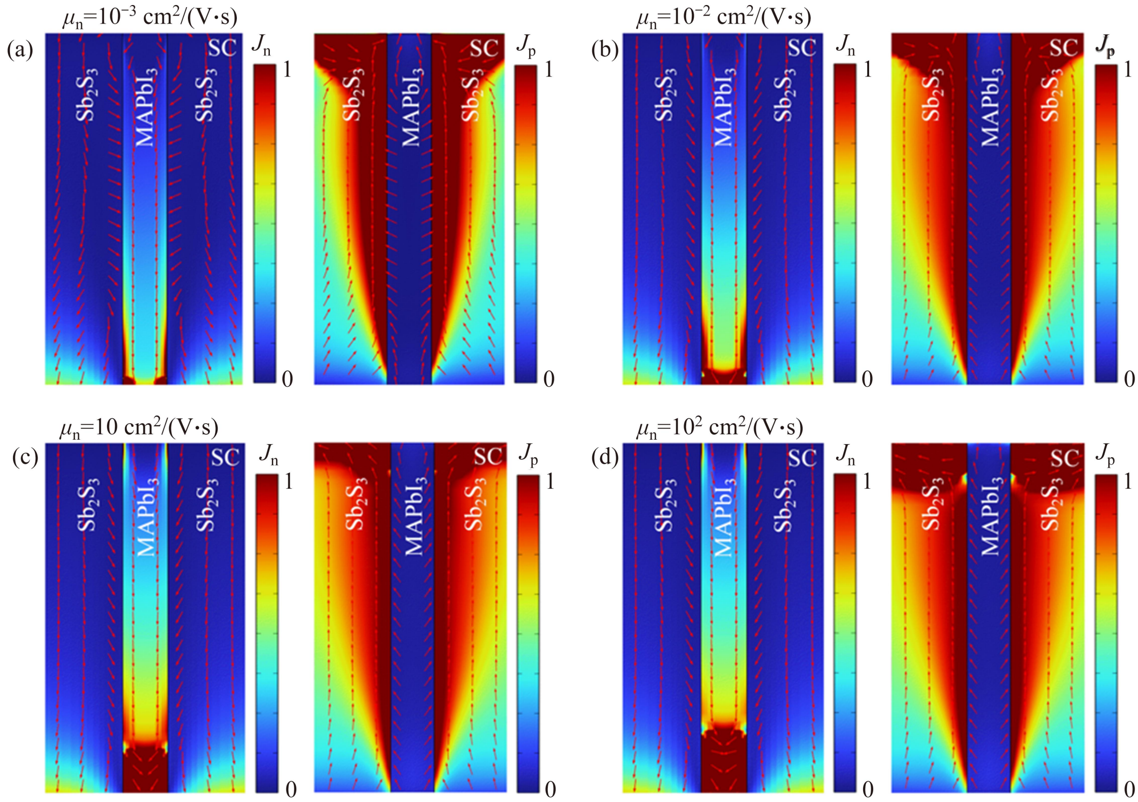

Figure S2 Electron and hole current density distributions under different electron mobilities: (a) 10^{-3} cm^2/(V·s); (b) 10^{-2} cm^2/(V·s); (c) 10 cm^2/(V·s); (d) 10^2 cm^2/(V·s) (μ_p=μ_n/2), where arrows denote the extraction directions of electrons and holes

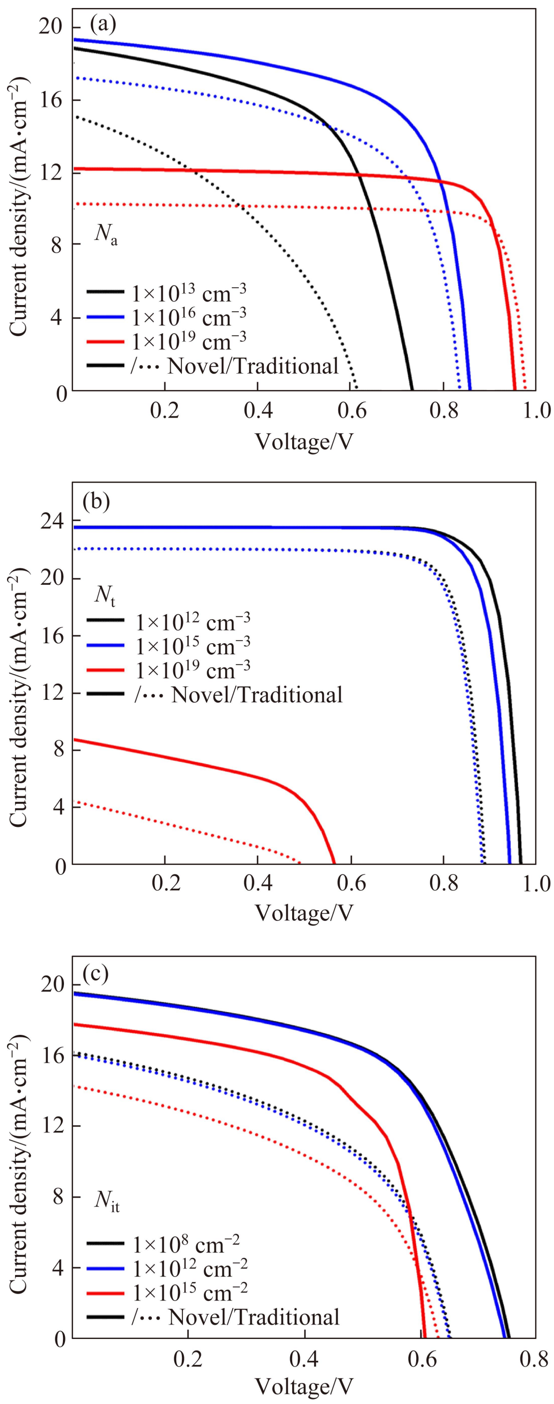

Figure S3 (a) $J-V$ curves under representative N_a values; (b) $J-V$ curves under representative N_t values; (c) $J-V$ curves under representative N_{it} values

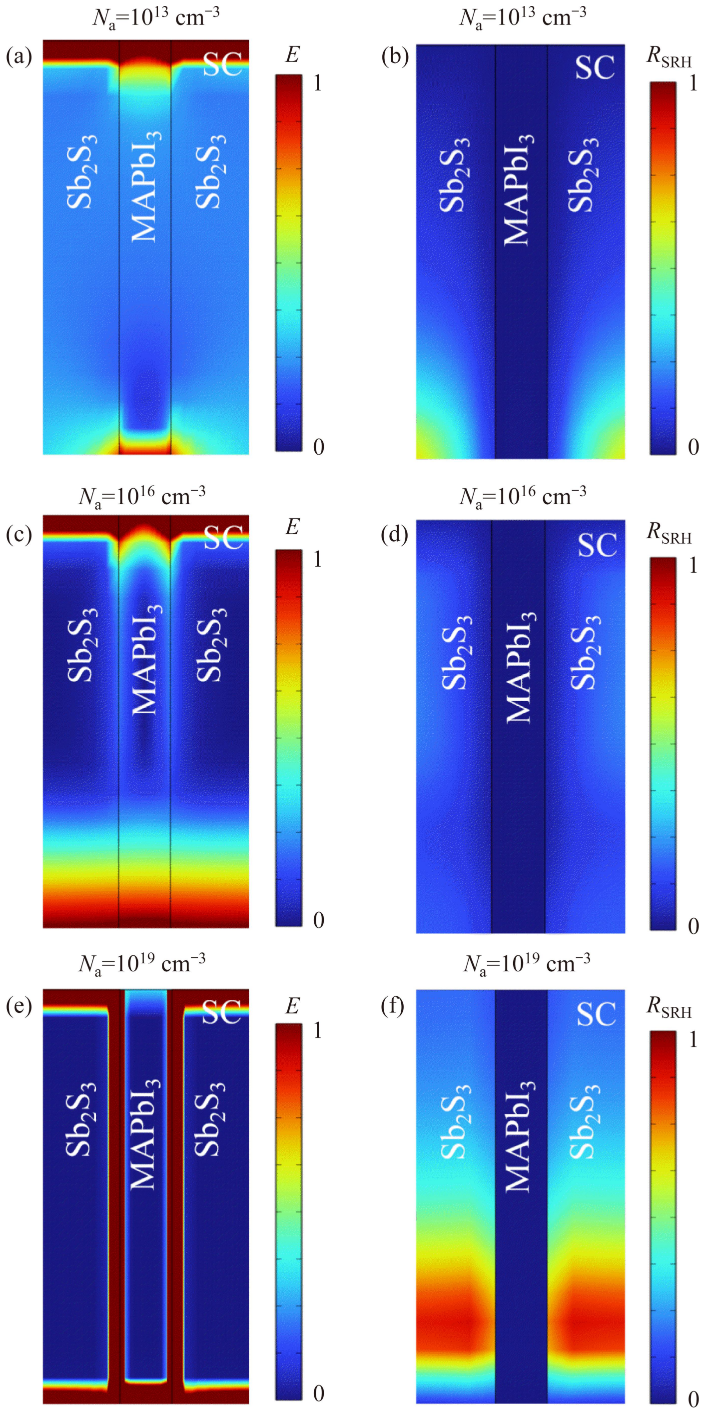

Figure S4 Distribution profiles of (a) electric field intensity (E) and (b) SRH recombination rate (R_{SRH}) in the novel Sb_2S_3 solar cell at N_a=10^{13} cm^{-3}; Distribution profiles of (c) electric field intensity and (d) SRH recombination rate in the novel solar cell at N_a=10^{16} cm^{-3}; Distribution profiles of (e) electric field intensity and (f) SRH recombination rate in the novel structure at N_a=10^{19} cm^{-3}

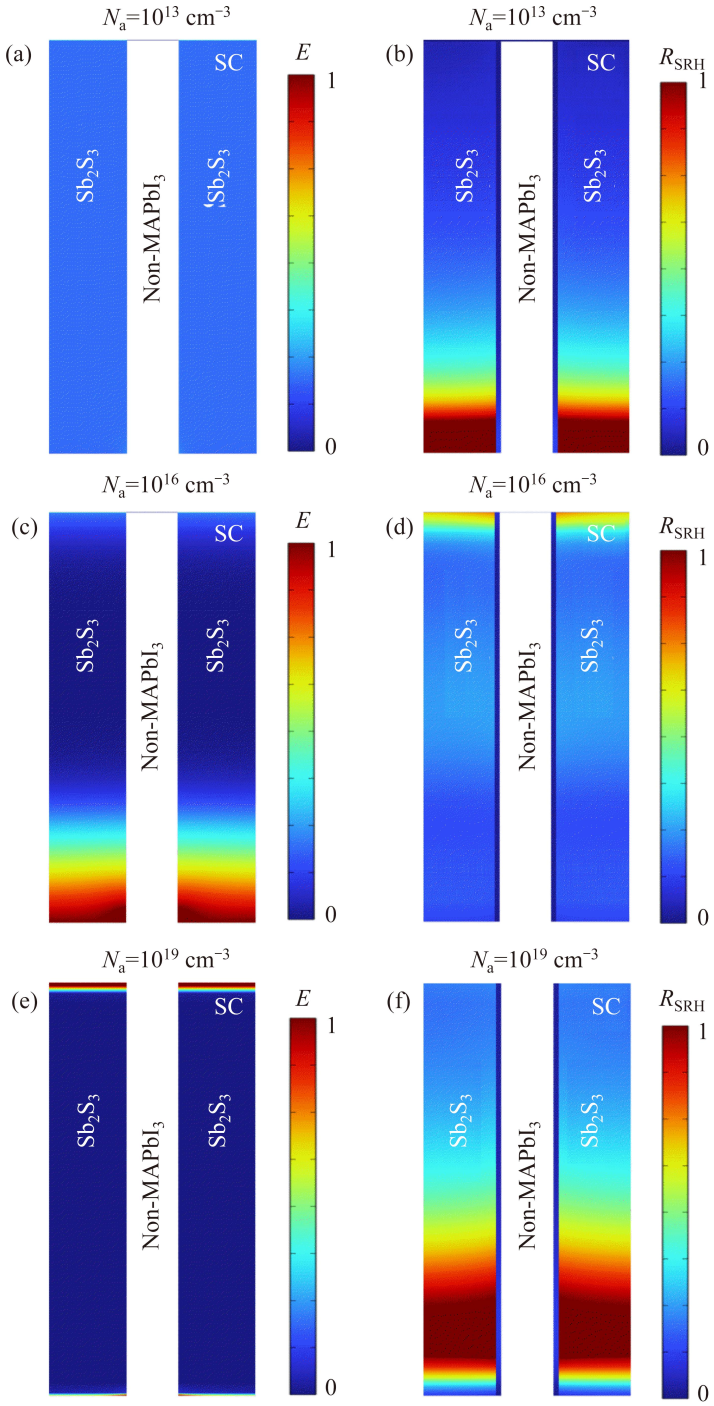

Figure S5 Distribution profiles of (a) electric field intensity and (b) SRH recombination rate in the traditional Sb_2S_3 solar cell at N_a=10^{13} cm^{-3}; Distribution profiles of (c) electric field intensity and (d) SRH recombination rate in the traditional Sb_2S_3 solar cell at N_a=10^{16} cm^{-3}; Distribution profiles of (e) electric field intensity and (f) SRH recombination rate in the traditional Sb_2S_3 solar cell at N_a=10^{19} cm^{-3}

The calculation formulas of photo-generated carriers

The photo-generated carriers rate $g(x, y, z, \lambda)$ in this model is expressed as follows [5]:

$$P_S(x,y,z,\lambda)=\sqrt{|P_{Sx}(x,y,z,\lambda)|^2+|P_{Sy}(x,y,z,\lambda)|^2+|P_{Sz}(x,y,z,\lambda)|^2} \tag{1}$$

$$P_{Sx}(x,y,z,\lambda)=\frac{1}{2}\mathrm{Re}(E_yH_z^*-E_zH_y^*) \tag{2}$$

$$P_{Sy}(x,y,z,\lambda)=\frac{1}{2}\mathrm{Re}(E_z H_x^* - E_x H_z^*) \tag{3}$$

$$P_{Sz}(x,y,z,\lambda)=\frac{1}{2}\mathrm{Re}(E_x H_y^* - E_y H_x^*) \tag{4}$$

where P_{Sx}, P_{Sy} and P_{Sz} are the power flux components in the x, y and z directions, respectively; E/H is the frequency and spatially dependent electric/magnetic field; 'Re' and '*' are the operators used to obtain the real component and the complex conjugate, respectively. Therefore, the spatially dependent generation (G) can be expressed as:

$$G(x,y,z)=\int_{\lambda_{\min}}^{\lambda_{\max}} g(x,y,z,\lambda)\mathrm{d}\lambda \tag{5}$$

In Eq. (6), $\lambda_{\min}$ and $\lambda_{\max}$ are the minimum and maximum values of the absorption wavelength, which were taken as 300 and 1200 nm, respectively.

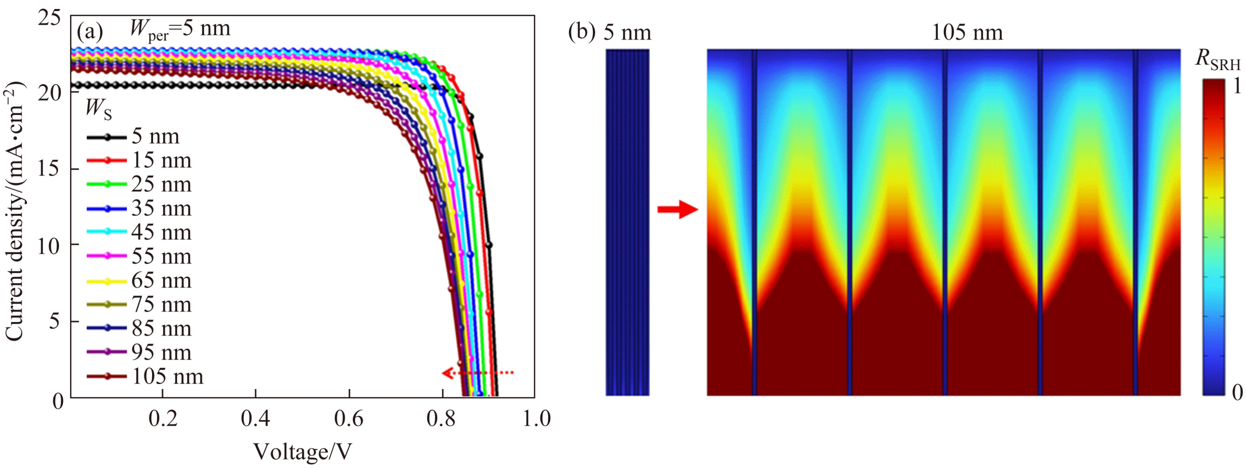

Figure S6 (a) J−V curves under varying Sb_2S_3 widths (W_S) with the perovskite width (W_{per}) fixed at 5 nm; (b) Evolution of the SRH recombination rate distribution as W_S increases from 5 nm to 105 nm

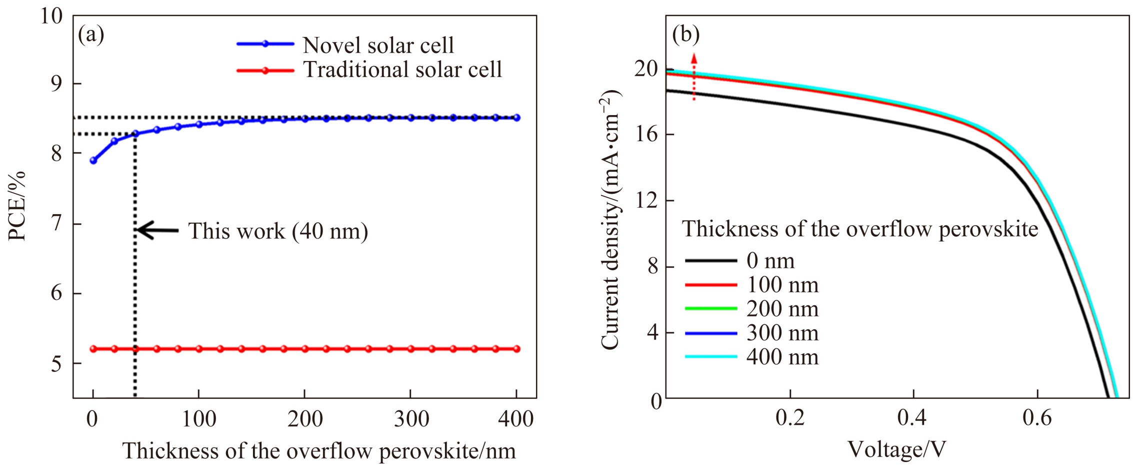

Figure S7 (a) PCE as a function of the excess perovskite layer thickness, and (b) the corresponding J−V curves

Table S2 Simulated PCE for different nanogap materials

Material	χ/eV	E_g/eV	PCE/%
C_{60}	3.9	1.7	6.64
PCBM	3.9	2	7.22
$MAPbI_3$	4.2	1.59	8.35
$CuSbS_2$	4.2	1.58	8.17
CuO	4.07	1.51	7.73
WS_2	3.95	1.8	6.84
$CsSnCl_3$	3.90	1.52	6.78
Sb_2S_3	3.7	1.65	6.13
ICBA	3.7	2	6.15

References

[1] LI Gui-jin, GUO Fang-fang, ZHOU Xi-lin, et al. Design and simulation of Sb_2S_3 solar cells based on monolayer graphene as electron transport layer [J]. Optical Materials, 2021, 112: 110791. DOI: 10.1016/j.optmat.2020.110791.

[2] LI Xiao-feng, HYLTON N P, GIANNINI V, et al. Multi-dimensional modeling of solar cells with electromagnetic and carrier transport calculations [J]. Progress in Photovoltaics: Research and Applications, 2013, 21(1): 109−120. DOI: 10.1002/pip.2159.

[3] HOSSAIN M K, TOKI G F I, KUDDUS A, et al. An extensive study on multiple ETL and HTL layers to design and simulation of high-performance lead-free $CsSnCl_3$-based perovskite solar cells [J]. Scientific Reports, 2023, 13(1): 2521. DOI: 10.1038/s41598-023-28506-2.

[4] ZHU Liang-xin, LIU Rong, WAN Zhi-yang, et al. Parallel planar heterojunction strategy enables Sb_2S_3 solar cells with efficiency exceeding 8% [J]. Angewandte Chemie International Edition, 2023, 62(50): e202312951. DOI: 10.1002/anie.202312951.

[5] ZANDI S, RAZAGHI M. Finite element simulation of perovskite solar cell: A study on efficiency improvement based on structural and material modification [J]. Solar Energy, 2019, 179: 298−306. DOI: 10.1016/j.solener.2018.12.032.